17th World Conference on Earthquake Engineering, 17WCEE
Sendai, Japan - September 13th to 18th 2020

Developing and Testing Earthquake Early Warning Parameters, τ_p^{max} and τ_c, for Rapid Magnitude Estimation in Southwestern China

H. Li[(1)], J. Zhang[(2)]

[(1)] *Ph.D. Student, University of Notre Dame, hli22@nd.edu*
[(2)] *Professor, Southwest Jiaotong University, jianjing.zhang@qq.com*

Abstract

Earthquake Early Warning system (EEWs) is one of the most effective ways for seismic hazard mitigation, in which predicting earthquake magnitude is one of the most important and difficult tasks. To mitigate the potential seismic disasters in southwestern China, building up the suitable magnitude estimation models for EEWs is very important. Currently, different empirical models have been used to estimate earthquake magnitude based on τ_p^{max} or τ_c derived by initial part of P-waves. In this paper, the records from the main- and after-shocks of the 2008 Wenchuan (M_w 7.9) and 2013 Lushan earthquakes (M_w 6.6), occurred in Sichuan region, were used to develop the maximum predominant (τ_p^{max}) and characteristic periods (τ_c) models for estimating earthquake magnitude. The τ_p^{max} parameter is correlated with magnitudes in the 4-6 range and 6-8 range, while τ_c parameter scales with the entire magnitude range without evident saturation. And then we do the further research and verify on rapid magnitude estimation model based on events in the Yunnan region in 2014. The result shows that these two frequency-based models can be effectively used for magnitude estimation in a short time window length. As for the database in this study, τ_p^{max}-3s and τ_c-4s models work better. However, at that moment it is difficult to get the accurate epicentral/ hypocentral distance in a short time window length. Hence, the frequency-based parameters, τ_p^{max} or τ_c, are recommended to apply in EEWs. Our works offer an insight into the feasibility of the EEWs in southwestern China.

Keywords: earthquake early warning; magnitude estimation; model testing; southwestern China

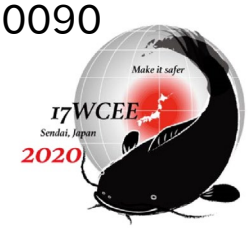

1. Introduction

21st century is a seismic active period in southwestern China. On 12 May, 2008, an earthquake of M_s 8.0 (M_w 7.9) shocked the Wenchuan County, Sichuan Province in China. The epicenter of this earthquake is 31.0°N, 103.4°E with the focal depth of 14 km and located in the mid-north of the Longmenshan Fault Zone (LFZ). Five years later, on 20 April, 2013, another large earthquake shocked the Lushan County, Sichuan again. The surface wave magnitude of the Lushan earthquake is 7.0 (M_w 6.6), its epicenter is 30.3°N, 103.0°E with the focal depth of 13 km and located in the south of the LFZ. Yunnan province, which also locates in the southwestern China and a high seismic risk area, has suffered three strong earthquakes with magnitude over 6.0 during four months in 2014. On 17 June, 2019, an M_s 6.0 earthquake hit the Changning County in Sichuan Province. During the following five days, strong aftershooks of M_s 5.1, M_s 5.3, M_s 5.4 occurred successively. On 4 July, 2019, another M_s 5.6 earthquake occurred in Gongxian County, Sichaun. These earthquakes caused great loss to people's lives and property.

Earthquake Early Warning system (EEWs) aims at providing seconds to tens of seconds to the target area for people to take emergency measures and reduce the loss before the arrival of destructive waves. Up till now, EEWs has been used in many countries and regions, such as Japan [1, 2, 3, 4, 5], Mexico [6], Romania [7], Turkey [8], Italy [9, 10], the United States [11, 12, 13] and Taiwan [14, 15], etc. Mainland China is no exception, after the 5-year testing of EEWs in Beijing capital region, in 2017 the government launched a 5-year program (total budget: 284 million US dollars) for establishing the EEWs based upon a densely seismic network of more than 15,000 seismic observatories in the whole country. Among the above applications, there are two types of EEWs, regional (network-based) and onsite (stand-alone) warning systems. For regional warning, the seismograph obtained from stations or arrays is used to estimate earthquake scale; for onsite warning, the seismograph used for identifying P-wave is from a single station and used for earthquake scale estimation. Generally, the regional warning has a higher accuracy than the onsite one because of the use of more stations and dense sensors arrays. However, different from Japan or California etc., up till the present moment, the seismic dense network has not been developed in China except for Beijing capital region. Hence, EEWs of developing based on single station, rather than network-based, is likely to be more valuable in southwestern region for the moment.

Among EEWs, the real-time magnitude estimation is one of the most important and difficult tasks. At present, seismologists have developed some of real time magnitude estimation parameters, like τ_p^{max}, τ_c, τ_{log}, P_d and $IV2$ [11, 16, 17, 18, 19, 20]. Furthermore, some methods or models for magnitude estimation are proposed, like the threshold-based method [17], evolutionary approach via inversion of displacement spectra [21] and the application of τ_c*P_d [22]. Until now, magnitude estimation algorithm in EEWs has not been developed in southwestern China, one of the largest seismic risk regions in China. It is worthy to perform study on developing and testing the parameters for rapid magnitude estimation in southwestern region.

In this study, we focus on the frequency-based magnitude estimation parameters, including τ_p^{max} and τ_c. And we use the earthquake records from the main- and after-shocks in the 2008 Wenchuan and 2013 Lushan earthquakes, which occurred in Sichuan region, to build up the τ_p^{max} and τ_c regression models for rapidly estimating earthquake magnitude. And then the models were evaluated for their performances on 2014 Yunnan earthquakes sequences.

2. Seismic Record Selections (Dataset)

937 earthquake records used to develop the magnitude estimation models, and 133 records used to test the models in this study are provided by China Strong Motion Network Centre (CSMNC), China Earthquake Administration. The training data include the main- and after-shocks of the M_w 7.9 Wenchuan earthquake (498 records) in 2008 and M_w 6.6 Lushan earthquake (439 records) in 2013. The testing data include the main- and after-shocks of M_W 5.9 Yingjiang earthquake (17 records) in 2014, M_W 6.2 Ludian earthquake (71 records) in 2014 and M_W 6.1 Jinggu earthquake (45 records) in 2014. The catalogue magnitudes are local magnitude M_L for events with $M_L < 6$ and moment magnitude M_w for larger events ($M_w \geq 6$) which are re-assigned using the CMT Harvard moment magnitude catalogue and denote both types of magnitudes simply by M in this study.

Both of the event location and magnitude have been revised. We set up three criteria of seismic record selections: 1) The magnitude of event is greater than 4.0; 2) To ensure good station coverage for each event and to avoid the near-source effect [23] and the complexity of path effects for P-waves at longer distances, the hypocentral distances are in the range of 20-100 km; 3) Only the vertical component of the record is used. Fig. 1 shows the distributions of the analyzed strong motion records (training data) as a function of magnitude and hypocentral distance.

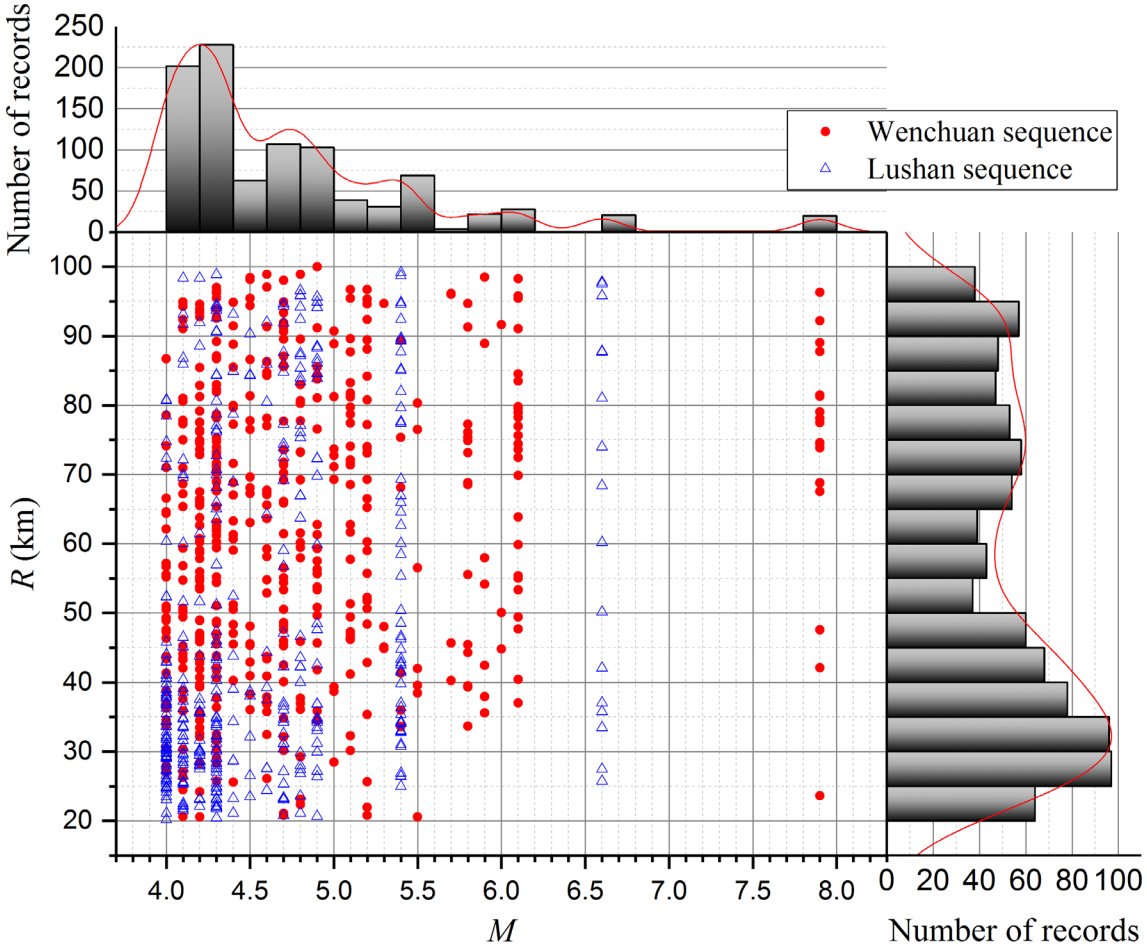

Fig. 1 - Distribution of training data as a function of magnitude and hypocentral distance

The P-arrivals from the vertical components and first S-arrivals from the horizontal components of all of the selected strong-motion records has been identified and manually picked, whose signal-to-noise ratio (SNR) are high enough to trace the P- and S-phase arrivals clearly. The S-picking is used to determine the longer P-phase time window to be used. The P-phase window shorter than 2 seconds are not commonly used since the parameter measures are affected by the trigger uncertainties, location error and amplitude bumps introduced by the filter. Hence, starting from the manually picked P-arrivals, we considered three different time window lengths, 2 s, 3 s and 4 s wide, on the 0.075 Hz high-pass filtered records where to measure the τ_p and τ_c.

Fig. 2a shows the acceleration waveform for three events that span the large magnitude ($M_w > 6$) with hypocentral distances nearly 70 km: the Wenchuan main event (M_w 7.9), the Lushan main event (M_w 6.6), and the Wenchuan main aftershock (M_w 6.1). The 2 s-P and 4 s-P phase windows are highlighted in gray before

the first S-phase arrival. Fig. 2b gives a simplified drawing for calculating τ_p^{max} and τ_c from one of the M_w 7.9 Wenchuan earthquake record which displayed in Fig. 2a at the same station.

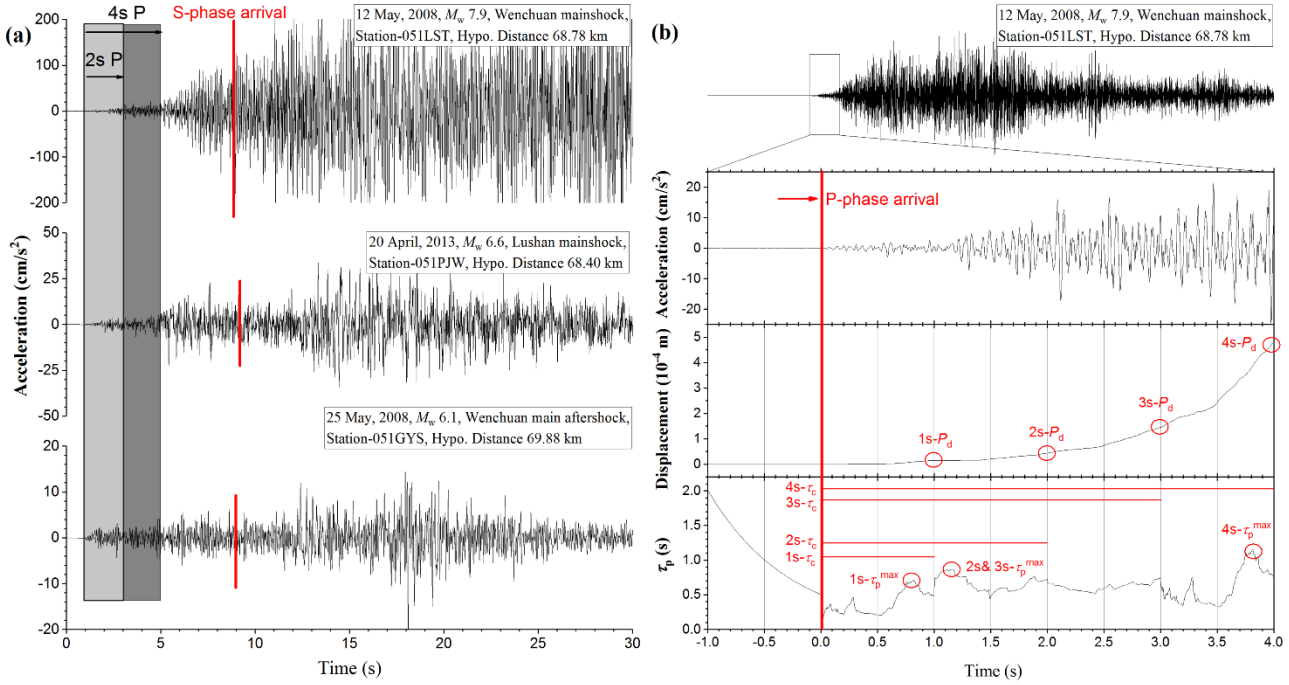

Fig. 2 (a) - The UD acceleration component for three large scale events of the investigated magnitude range. (b) - Example of calculating τ_p^{max} and τ_c.

3. Establishment of Parameters versus Magnitude Correlation (Model Developing)

3.1 Maximum of Predominant Period, τ_p^{max}

In 1988, Nakamura put forward the algorithm to calculate the seismic predominant period based on real-time velocity records, which has been applied to the Japanese Shinkansen EEW system, called UrEDAS [2]. Allen and Kanamori believed that the maximum of $\tau_p(i)$ calculated based on a few seconds after the arrival of the P-wave is proportional to earthquake magnitude, and so developed an algorithm, called τ_p^{max} method [11], as shown in Eq. (1). This method has been applied to California EEWs [24] and ElarmS system [14]. It should be noted that the correlation between τ_p^{max} and the strong event magnitude ($M_w > 6$) is not related only to the source properties, but it derives from a combination of attenuation, site effect and filtering effects [25, 26].

$$\tau_p(i) = 2\pi\sqrt{X_i/D_i} \tag{1}$$

where $X_i = \alpha X_{i-1} + x_i^2$ and $D_i = \alpha D_{i-1} + (dx/dt)_i^2$, x_i is the vertical velocity signal and α is a smoothing constant which is set as 0.999 in this study.

Using the recursive definition given in Eq. (1), we compute τ_p^{max} for the seismic records in our dataset and correlate with magnitude based on Eq. (2) in time window lengths of 2 s, 3 s and 4 s after P-arrival. The data have been high-pass-filtered at 0.075 Hz using 2-pole Butterworth filter. The computed result is shown in Fig. 3 while the detail of correlated result is reported in Table 1.

$$\log(\tau_p^{max}) = aM + b \tag{2}$$

where τ_p^{max} is maximum of $\tau_p(i)$, M denotes the catalogue magnitude and a, b represent constants determined by regression best fitting.

The best fitting regression equations for each time window length can be obtained based regression analysis. Fig. 3a-c show the results of fitting the data in different time window lengths (2 s, 3 s and 4 s). The τ_p^{max} parameter shows a large dispersion in the entire magnitude range. Since there are different numbers of seismic records for each earthquake bin, the mean values (the triangles in figures) are used to get the fitting line, which was also used by Allen & Kanamori [11] and Kanamori [16] to get a smaller deviation. The τ_p^{max} parameters are correlated with magnitudes in the 4.0-6.0 range and 6.0-8.0 range, however with the large overall standard error especially in the large magnitude. It clearly scales with the final magnitude in the 4.0-6.0 range, optimally in 3 s. Nevertheless, for magnitude higher than 6, it shows a weak dependence on the magnitude and evident underestimation with the lower-slope. Because of the large weighted standard error and statistical insignificance, the regression in M 6.0-8.0 range is not considered. τ_p^{max} saturates on M_w 6.0 in our dataset. The similar phenomenon appears in the values retrieved for Chile data [27] with the similar slope. With the increasing of time window length (longer than 3 s), the saturation improves slightly, but the parameters in the 4.0-6.0 range disperse in 4 s. The scatter might be attribute to the accumulation of small amount of low-frequency noise with the accumulated X and D term in Eq. (1). Based on comparing the correlation coefficients, the best fitting regression equation for the τ_p^{max} in this study is:

$$\text{mag 4-6: } \log(\tau_p^{max}) = (0.238 \pm 0.010)\, M - 1.489 \pm 0.056,$$
$$\text{or } M = 4.202 \log(\tau_p^{max}) + 6.256 \pm 0.235 \quad (3)$$

in the time window length of 3 s and with correlation coefficient of 0.97.

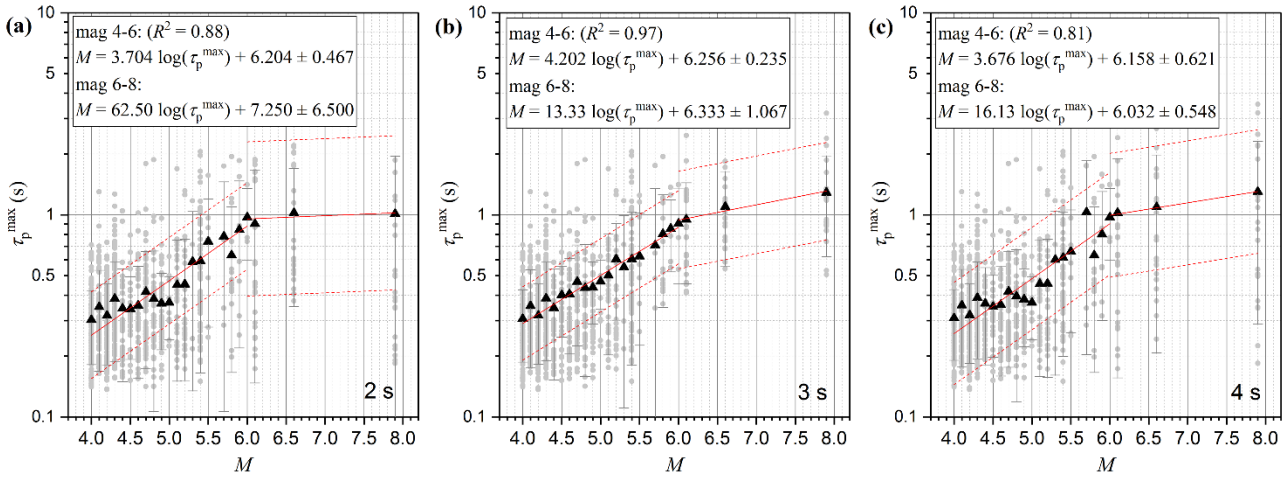

Fig. 3 - Correlation between τ_p^{max} and catalogue magnitude for time window length of (a) 2 s, (b) 3 s and (c) 4 s. The gray dots are the τ_p^{max} calculated from each record, while the triangles represent the average value of τ_p^{max} on each magnitude bin (associated standard deviation bars are included), which are used to do regression. Each panel shows the best fit regression line (solid line) along with 1-WSE limits (dashed lines) on the magnitude ranges of 4–6 and 6–8. The weighted standard error (WSE) is computed as $WSE = \sqrt{\frac{1}{n-1}\sum_{i=1}^{n}[\log(\tau_p^{max})_i - aM_i - b]^2}$ (a and b are the best-fit line parameters, which can be referred from Table 1 in details).

Table 1 - τ_p^{max} versus Magnitude

Magnitude	2 s P Phase		3 s P Phase		4 s P Phase	
	a ± Δa	b ± Δb	a ± Δa	b ± Δb	a ± Δa	b ± Δb
4.0-6.0	0.270 ± 0.023	-1.675 ± 0.126	0.238 ± 0.010	-1.489 ± 0.056	0.272 ± 0.031	-1.675 ± 0.169
6.0-8.0	0.016 ± 0.016	-0.116 ± 0.104	0.075 ± 0.012	-0.475 ± 0.080	0.062 ± 0.005	-0.374 ± 0.034

3.2 Characteristic Period, τ_c

In 2005, Kanamori improved the τ_p^{max} method and put forward the τ_c parameter by adopting the fixed interval integration instead of the original step by step integration [16]. The value of τ_c indicates the average of the periods within t seconds after the arrival of P-wave in the vertical component, as shown in Eq. (4). Currently this model has been applied to Virtual Seismologist system [28]. τ_c has the similar physical meaning with τ_p^{max}, but they perform different results for the same seismic record, which might be related to the noise level before the P-phase arrival [29].

$$\tau_c = 2\pi / \sqrt{r} = 2\pi / \sqrt{[\int_0^t \dot{u}^2(t)dt] / [\int_0^t u^2(t)dt]} \tag{4}$$

where $u(t)$ is the vertical displacement and t is the time window length.

Based on the recursive definition given in Eq. (4), we compute τ_c and correlate with magnitude by Eq. (5) in several time window lengths (2 s, 3 s and 4 s after P-arrival). The record has been high-pass-filtered at 0.075 Hz using 2-pole Butterworth filter. The computed result is shown in Fig. 4 while the detail of correlated result is reported in Table 2.

$$\log(\tau_c) = aM + b \tag{5}$$

where τ_c is the computed parameter, M denotes the catalogue magnitude and a, b represent constants determined by regression best fitting.

Fig. 4a-c show the results for fitting the data in time window lengths of 2 s, 3 s and 4 s, respectively. Unlike τ_p^{max} parameter, τ_c clearly scales with the entire magnitude range (4.0-8.0 range) with the larger overall standard error in 2 s and 3 s. It should be noted that the evident saturation does not occur. The discreteness becomes smaller as time window length increasing to 4 s. Nevertheless, the slope of 0.161 ± 0.012 is slightly lower than the values retrieved for the Japan, California and Taiwan datasets [16] and for the Chile datasets [27]. The lower slope implies the less sensitivity of τ_c for the change of magnitude, meaning that the less predictive for the larger magnitude. Based on comparing the correlation coefficients, the best fitting τ_c regression equation for our dataset is:

$$\text{mag 4-8: } \log(\tau_c) = (0.161 \pm 0.012)\, M - 0.768 \pm 0.072,$$
$$\text{or } M = 6.211 \log(\tau_c) + 4.770 \pm 0.447 \tag{8}$$

in the time window length of 4 s and with correlation coefficient of 0.87.

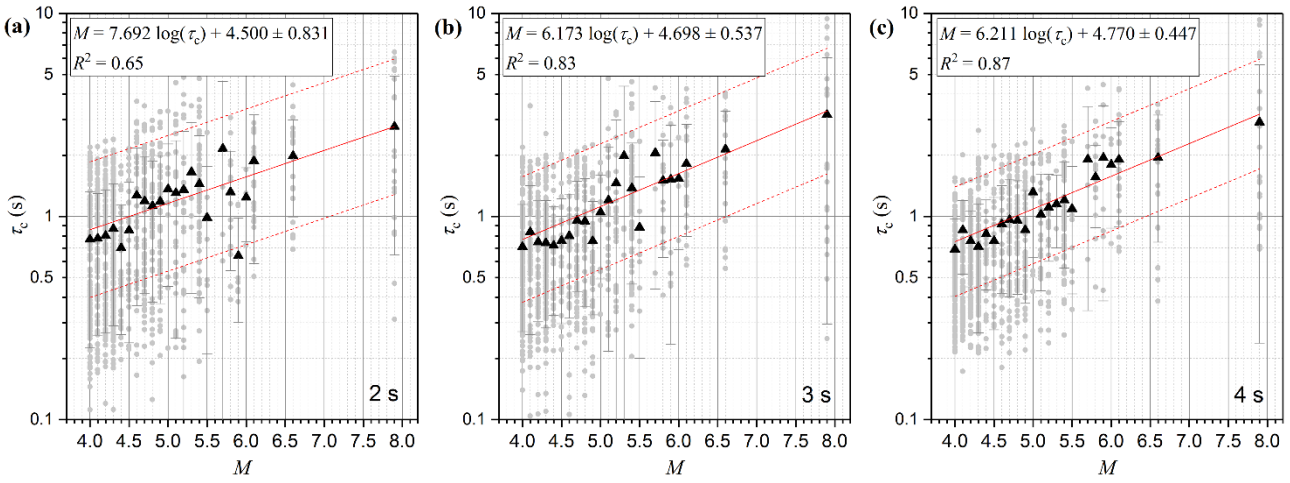

Fig. 4 - Correlation between τ_c and catalogue magnitude for time window length of (a) 2 s, (b) 3 s and (c) 4 s. The gray dots are the τ_c calculated from each record, while the triangles represent the average value of τ_c on

each magnitude bin (associated standard deviation bars are included), which are used to do regression. Each panel shows the best fit regression line (solid line) along with 1-WSE limits (dashed lines) on the magnitude ranges of 4–8.

Table 2 - τ_c versus Magnitude

	2 s P Phase		3 s P Phase		4 s P Phase	
Magnitude	a ± Δa	b ± Δb	a ± Δa	b ± Δb	a ± Δa	b ± Δb
4.0-8.0	0.130 ± 0.018	-0.585 ± 0.108	0.162 ± 0.014	-0.761 ± 0.087	0.161 ± 0.012	-0.768 ± 0.072

4. Parameters Application (Model Testing)

The applicability of the above models were evaluated for their performances as magnitude estimators based on the dataset that compose from the main- and after-shocks of Yingjiang earthquake (M_W 5.9), Ludian earthquake (M_W 6.2) and Jinggu earthquake (M_W 6.1) in Yunnan region in 2014. Fig. 5 shows the distributions of the analyzed strong motion records (testing data) as a function of magnitude and hypocentral distance.

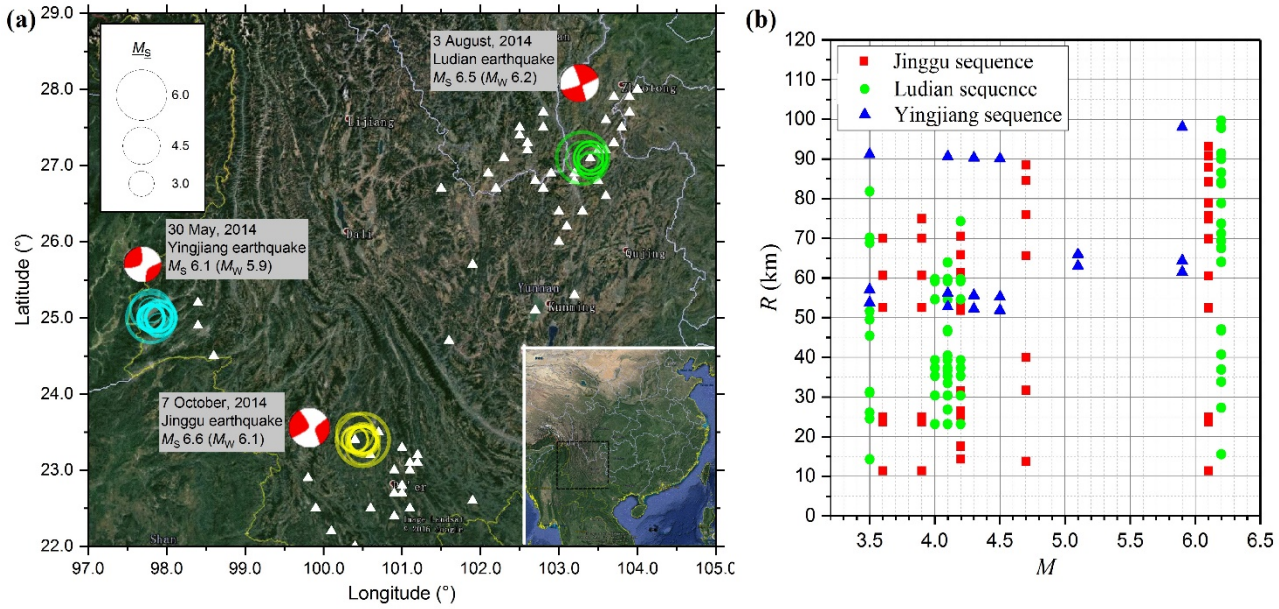

Fig. 5 (a) - Map of the locally permanent stations (solid triangles) in Yunnan region and events used for model testing. (b) - Distribution of the testing data as a function of the catalogue magnitude and hypocentral distance.

Based on the dataset, the frequency-based parameters with the time windows of 2 s, 3 s and 4 s are calculated by Eq. (1) and (4). Then, the corresponding estimated magnitude is obtained by substituting them into the corresponding magnitude estimation model of Sichuan region in different time window lengths. The applicability of these models with different time window length can be evaluated based on the residual analysis.

Fig. 6a-c show the relationship between the catalog magnitude and the estimated magnitude calculated by the τ_p^{max} estimation models with the time windows of 2 s, 3 s and 4 s, respectively. For the overall data, the estimated magnitudes have great discreteness. We can effectively reduce the error by obtaining the mean value for the same event. For time window length of 2 s, the average absolute error of the estimated magnitude is 0.41 magnitude unit while the standard deviation is 0.20 magnitude unit. The residuals of estimated magnitudes of 16 events are all within ± 1.0 magnitude unit, and 10 of them are within ± 0.5 magnitude unit. For time window length of 3 s, the average absolute error of the estimated magnitude is 0.37 magnitude unit with 0.19 magnitude unit standard deviation. The residuals of estimated magnitudes of 16 events are all within ± 1.0

magnitude unit, and 12 of them are within ± 0.5 magnitude unit. For the time window length of 4 s, the average absolute error of the estimated magnitudes is 0.53 magnitude unit with the standard deviation of 0.26 magnitude unit. The residuals of estimated magnitudes of 16 events are all within ± 1.0 magnitude unit, and 7 of them are within ± 0.5 magnitude unit. τ_p^{max} estimation model with 3 s time window performs better than 4 s time window length. It might be attribute to the accumulation of small amount of low-frequency noise with the accumulated X and *D* term in Eq. (1).

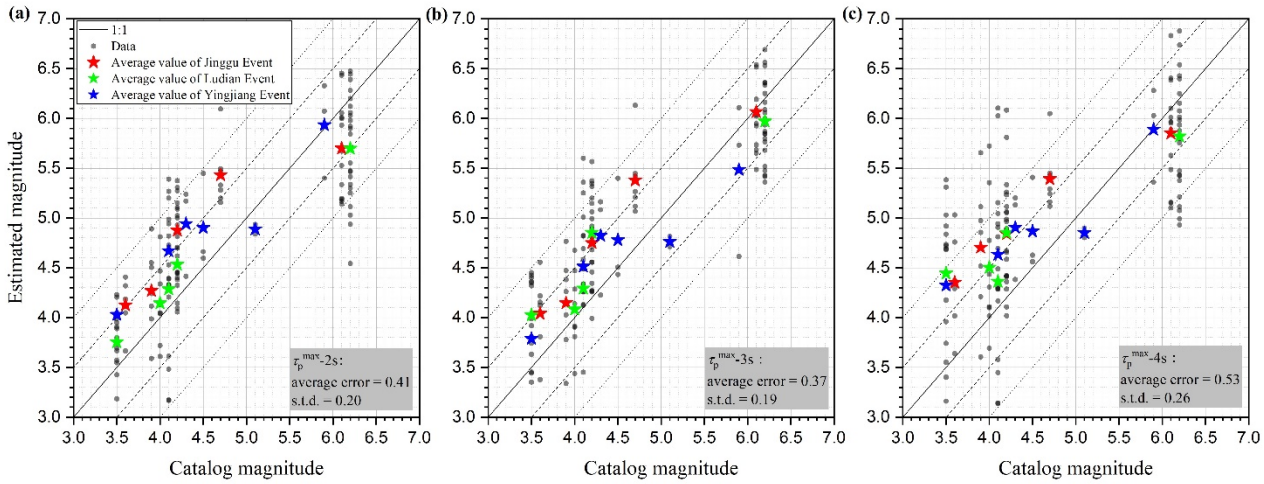

Fig. 6 - The relationship between the catalog magnitude and the estimated magnitude calculated by the τ_p^{max} estimation models with the time windows of (a) 2 s, (b) 3 s and (c) 4 s.

Different from τ_p^{max} parameter, Fig. 7a-c show that τ_c parameter performs worse in the short time window length (2 s or 3 s) with large error and discreteness, however, it performs better when the window length increases (4 s). For time window length of 4 s, the average absolute error of estimated magnitude is 0.26 magnitude unit, and the standard deviation is 0.30 magnitude unit. The residuals of estimated magnitude of 16 events are all within ± 1.0 magnitude unit, and 12 of them are within ± 0.5 magnitude unit. It should be noted that the average error is slightly less than τ_p^{max} parameter with 3 s time window length, but the discreteness is slightly greater. This may be related to the smaller slope of the fitting line of the τ_c magnitude estimation model, which means that the parameter is relatively insensitive to the magnitude change.

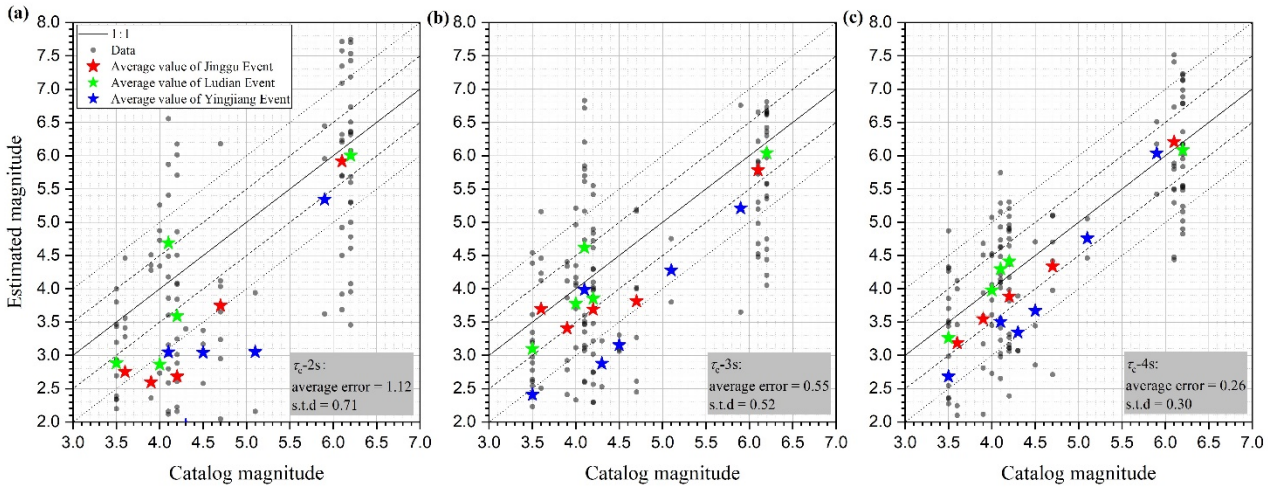

Fig. 7 - The relationship between the catalog magnitude and the estimated magnitude calculated by the τ_c estimation models with the time windows of (a) 2 s, (b) 3 s and (c) 4 s.

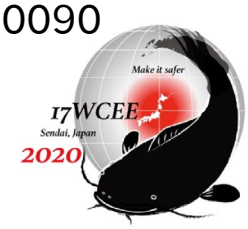

5. Conclusion and Discussions

In this study, we focused on two frequency-based parameters proposed for the real-time magnitude estimation for EEWs application in southwestern China: maximum of predominant period (τ_p^{max}) and characteristic period (τ_c). We develop the magnitude estimation model of those parameters on the sequence of the main- and after-shocks in the 2008 Wenchuan (M_w 7.9) and 2013 Lushan (M_w 6.6) events in Longmenshan fault zone (LFZ), Sichuan region. And we investigated the performance of those models on the sequence of the main- and after-shocks in the 2014 Jinggu (M_w 6.1) and 2014 Ludian (M_w 6.2) and 2014 Yingjiang (M_w 5.9) events in Yunnan region.

Firstly, we constructed the dataset by several criteria from China Strong Motion Network Centre (CSMNC), China Earthquake Administration, in which the main- and after-shocks of the Wenchuan earthquake (498 records) and Lushan earthquake (439 records) are included. We manually determined their P-wave arrivals and first S-wave arrivals with high signal-to-noise ratio (SNR).

The second part of this study was the investigation of the correlation between the τ_p^{max}, τ_c parameters and the catalogue magnitude in different short time window length. As a result, the τ_p^{max} parameter is severally correlated with magnitudes in the 4.0-6.0 range and 6.0-8.0 range, with the large overall standard error and smaller linear slope especially in the large magnitude. Unlike τ_p^{max}, τ_c parameter scales with the entire magnitude range (4.0-8.0 range) without evident saturation. Nevertheless, the linear slope is slightly lower than the values retrieved for the Japan, California and Taiwan datasets [16] and for the Chile data [27].

Finally, the two parameter regression models are evaluated by the testing data. The results show that both of two magnitude estimation parameters are practical and can effectively estimate the magnitude based on the testing dataset in a short time window length (3 s or 4 s). τ_p^{max} -3s and τ_c -4s models perform better than the other models with different time window length. It should be noted that both of these frequency-based parameters are hypocenter distance independent.

This study open a new perspective on the feasibility of EEWs in southwestern China, one of the largest seismic risk regions. After the 5-years testing of EEWs in Beijing capital region, the development of EEWs in southwestern region is in progress, and it is imperative. In present, the source distance cannot be quickly and accurately obtained by using real-time location procedures as, for instance, the method proposed by *Horiuchi et al.*[30] without the seismic dense network. Hence, we recommended the distance-independent parameters to estimate the earthquake magnitude in EEWs practical application for the moment. Moreover, to develop EEWs in a specific region, it is necessary to consider the regional characteristics and propose the suitable regression model (the optimal time window length) for the given region. The ultimate ideal is to prefigure the real-time alert system operating in the seismic risk region or vital region (such as Longmenshan region and Beijing capital region) based on the continuous time evolution [31].

6. Acknowledgement

The strong-motion records used in the present study were kindly provided by the China Strong Motion Network Centre (CSMNC) of China Earthquake Administration for making the strong motion data accessible through website http://www.csmnc.net/ (last accessed in June 2016), but they are not publicly available. We acknowledge the CSMNC of China Earthquake Administration for making the strong motion data access. The authors wish to appreciate Editors and Reviewers very much for their positive and constructive comments and suggestions on this manuscript.

7. References

[1] Nakamura, Y. (1984): Development of earthquake early-warning system for the Shinkansen, some recent earthquake engineering research and practical in Japan, *The Japanese National Committee of the International Association for Earthquake Engineering*, 224-238.

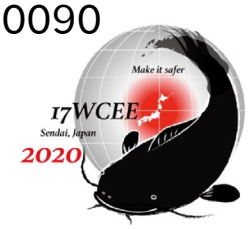

[2] Nakamura, Y. (1988): On the urgent earthquake detection and alarm system (UrEDAS), *Proceedings of 9th World Conference on Earthquake Engineering*, Vol. VII, 673-678.

[3] Odaka, T., Ashiya, K., Tsukada, S., Sato, S., Ohtake, K., Nozaka, D. (2003): A new method of quickly estimating epicentral distance and magnitude from a single seismic record, *Bull. seism. Soc. Am.*, **93**, 526-532.

[4] Kamigaichi, O. (2004): JMA earthquake early warning. *Assoc. Earthquake Eng*. **4** (3), 134-137.

[5] Horiuchi, S., Negishi, H., Abe, K., Kamimura, A., Fujinawa, Y. (2005): An automatic processing system for broadcasting system earthquake alarms, *Bull. sesim. Soc. Am.*, **95**, 347-353.

[6] Espinosa-Aranda, J.M., Cuellar, A., Garcia, A., Ibarrola, G., Islas, R., Maldonado, S., Rodriguez, F.H. (2009): Evolution of the Mexican Seismic Alert System (SASMEX), *Seism. Res. Letters*, **80** (5), 694–706.

[7] Bose, M., Ionescu, C., Wenzel, F. (2007): Earthquake early warning for Bucharest, Romania: novel and revised scaling relations, *Geophys. Res. Lett.*, **34** (7).

[8] Alcik, H., Ozel, O., Apaydin, N., Erdik M. (2009): A study on warning algorithms for Instabul earthquake early warning system, *Geophys. Res. Lett.*, **36**, L00B05.

[9] Zollo, A., Lancieri, M., Nielsen, S. (2006): Earthquake magnitude estimation from peak amplitudes of very early seismic signals on strong motion, *Geophys. Res. Letters*, **33**, L23312.

[10] Zollo, A., Iannaccone, G., Lancieri, M., Cantore, L., Convertito, V., Emolo, A., Festa, G., Gallovic, F., Vassallo, M., Martino, C., Satriano, C., and Gasparini, P. (2009): Earthquake early warning system in southern Italy, *Geophys. Res. Letters*, **36** (5), 121-136.

[11] Allen, R.M., Kanamori, H. (2003): The potential for earthquake early warning in Southern California, *Science*, **300** (5620), 786–789.

[12] Allen, RM., Gasparini, P., Kamigaichi, O., Böse, M. (2009): The status of earthquake early warning around the world: An introductory overview, *Seismol. Res. Lett.*, **80** (5), 682–693.

[13] Bose, M., Hauksson, E., Solanki, K., Kanamori, H., Heaton, T.H. (2009): Real-time testing of the on-site warning algorithm in southern California and its performance during the July 29, 2008 Mw 5.4 Chino Hills earthquake, *Geophys. Res. Lett.*, **36**, L00B03.

[14] Wu, Y.M., Kanamori, H. (2005): Experiment on an onsite early warning method for Taiwan early warning system, *Bull. Seismol. Soc. Am.*, **95**, 347-353.

[15] Hsiao, N.C., Wu, Y.M., Shin, T.C., Zhao, L., Teng, T.L. (2009): Development of earthquake early warning system in Taiwan, *Geophys Res Lett*, L00B02, **36** (2), 436-448.

[16] Kanamori, H. (2005): Real-time seismology and earthquake damage mitigation. *Annu Rev Earth Pl Sci*, **33**, 195-214.

[17] Zollo, A., Amoroso, O., Lancieri, M., Wu, Y.M., Kanamori, H. (2010): A threshold-based earthquake early warning using dense accelerometer networks, *Geophys J Int*, **183**, 963–974.

[18] Ziv, A. (2014): New frequency-based real-time magnitude proxy for earthquake early warning, *Geophys. Res. Lett.*, **41**, 7035–7040.

[19] Wu, Y. M., Yen, H., Zhao, L., Huang, B., Liang, W. (2006): Magnitude determination using initial P waves: A single-station approach, *Geophys. Res. Lett.*, **33**, L05306.

[20] Festa, G., Lancieri, M., Zollo, A. (2008): Magnitude estimation from early radiated energy, *Geophys Res Lett*, **35**, L22307.

[21] Caprio, M., Lancieri, M., Cua, G. B., Zollo, A., Wiemer, S. (2011): An evolutionary approach to real-time moment magnitude estimation via inversion of displacement spectra, *Geophys. Res. Lett.*, **38**, L02301.

[22] Huang, P.L., Lin, T.L., Wu, Y.M. (2015): Application of τc*Pd in earthquake early warning, *Geophys. Res. Lett.*, **42**, 1403–1410.

[23] Yamada, M., Mori, J. (2009): Using τ_c to estimate magnitude for earthquake early warning and effects of near-field terms, J. Geophys. Res., **114**, B05301.

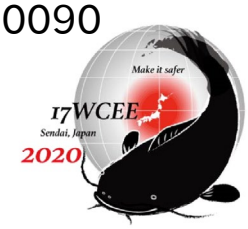

[24] Wurman, G., Allen, R.M., Lombard, P. (2007): Toward earthquake early warning in northern California, *Journal of Geophysical Research*, **112**, B08311.

[25] Wolfe, C. (2006): On the properties of predominant-period estimators for earthquake early warning, *Bull. Seismol. Soc. Am*. **96** (5), 1961–1965.

[26] Yamada, T., Ide, S. (2008): Limitation of the predominant-period estimator for earthquake early warning and the initial rupture of earthquakes, *Bull. Seismol. Soc. Am*. **98** (6), 2739–2745.

[27] Lancieri, M., Fuenzalida, A., Ruiz, S., Madariaga, R. (2011): Magnitude Scaling of Early-Warning Parameters for the M_w 7.8 Tocopilla, Chile, Earthquake and Its Aftershocks, *Bull. Seismol. Soc. Am*., **101** (2), 447-463.

[28] Cua, GB., Fischer, M., Heaton, T., Wiemer. (2009): Real-time performance of the Virtual Seismologist earthquake early warning algorithm in Southern California, *Seismol. Res. Lett*., **80** (5), 740–747.

[29] Shieh, J., Wu, Y.M., and Allen, R.M. (2008): A comparison of τ_c and τ_p^{max} for magnitude estimation in earthquake early warning, *Geophys. Res. Lett*. **35**, L20301.

[30] Horiuchi, S., Negishi, H., Abe, K., Kamimura, A., Fujinawa, Y. (2005): An automatic processing system for broadcasting system earthquake alarms, *Bull. sesim. Soc. Am*., **95**, 347–353.

[31] Colombelli, S., Zollo, A. (2016): Rapid and reliable seismic source characterization in earthquake early warning systems: current methodologies, results, and new perspectives, *J. Seismol*, **20**, 1171–1186.

